

Reinforced Evolutionary Neural Architecture Search

Yukang Chen^{1*} Qian Zhang² Chang Huang² Lisen Mu² Gaofeng Meng¹ Xinggang Wang³

¹National Laboratory of Pattern Recognition, Institute of Automation, Chinese Academy of Science

²Horizon Robotics ³Huazhong Univ. of Science and Technology

{chenyukang2017@, gfmeng@nlpr.}ia.ac.cn

{qian01.zhang, chang.huang, lisen.mu}@horizon.ai, {xgwang}@hust.edu.cn

Abstract

Neural architecture search (NAS) is an important yet challenging task in network design due to its high computational consumption and low stability. To address these two issues, we propose the Reinforced Evolutionary Neural Architecture Search (RENAS), which is an evolutionary method with reinforced mutation for NAS. Our method integrates reinforced mutation into an evolution algorithm for neural architecture exploration, in which a mutation controller to learn the effects of slight modifications and make mutation actions. The reinforced mutation controller instructs the model population to evolve efficiently in a suitable direction. Furthermore, as child models can inherit parameters from their parents during evolution, our method requires very limited computational resources. We conduct the proposed search method on CIFAR-10 with 4 GPUs (Titan Xp) across 1.5 days and discover a powerful network architecture. This architecture achieves a competitive result on CIFAR-10. We further apply the explored network architecture to the mobile setting ImageNet. The network achieves a new state-of-the-art accuracy, i.e., 75.7% top-1 accuracy with 5.36M parameters.

Introduction

Recent several years have witnessed the great success of neural networks (Szegedy et al. 2015; He et al. 2016; Szegedy et al. 2016; 2017; Huang et al. 2017) in tackling various challenging tasks, e.g., image classification, object detection and semantic segmentation. However, designing hand-crafted neural networks is still a laborious task due to the heavy reliance on expert experience and large amount of trials. For example, hundreds of experts in academia and industry have made great efforts to optimize the architectures of neural networks to increase the top-5 accuracy on ImageNet challenge to 96.43% from AlexNet (Krizhevsky, Sutskever, and Hinton 2012), VGG (Simonyan and Zisserman 2014), Inception (Szegedy et al. 2015) to ResNet (He et al. 2016).

Techniques in automatically designing network architectures have attracted increasing research interests. Many neural architecture search (NAS) methods have been proposed and proven to be capable of yielding high-performance models. A large portion of these methods are based on Reinforcement Learning (RL) (Zoph et al. 2017; Cai et al. 2018;

Zoph and Le 2016; Zhong et al. 2018) or Evolution Algorithm (EA) (Real et al. 2018; Stanley and Miikkulainen 2002; Real et al. 2017; Miikkulainen et al. 2017; Xie and Yuille 2017). The typical RL-based NAS methods construct networks sequentially, e.g., by using a RNN controller (Zoph et al. 2017; Pham et al. 2018; Zoph and Le 2016) to output a sequence of operator and connection tokens. In EA-based NAS methods, a population of models is initialized and then evolve with their validation accuracies as fitnesses.

EA and RL have produced competitive models and even achieved the state-of-the-art performance. However, several issues still remain unsolved: 1) For EA-based NAS, we empirically find the search stability is fragile. Uncontrollable random mutation often leads to instability or even breakdown in neural architecture search. This severely degrades the final results. 2) For RL-based NAS, the search efficiency can not be guaranteed. When deciding a model layer by layer, the RL controller needs to make tens of actions to get a reward. This makes the training process sample-wise inefficient.

In this paper, we propose the Reinforced Evolutionary Neural Architecture Search (RENAS), which integrates RL into the evolution framework to address the above issues. Our method introduces a reinforced mutation controller to help the stable and efficient exploration of the search space. Thanks to the nature of EA, the child model could inherit most parameters from its parent, which in turn makes the search much efficient.

Our main contributions are summarized as below:

- A novel neural architecture search framework is proposed with EA and RL integrated. This framework achieves better search stability than the common EA based NAS and it is more efficient than most methods.
- We design a reinforced mutation controller to learn the effects of slight modifications and make mutation actions to instruct the evolution. This technique helps the population evolve to a better status in fewer iterations and avoid the harm of uncontrollable random mutations.
- A powerful network architecture is discovered with only 4 GPUs in 1.5 days. It achieves a competitive accuracy on CIFAR-10, i.e. $2.98\% \pm 0.08$. We also test the explored network architecture on the mobile setting ImageNet and it achieves a new state-of-the-art on the dataset with 75.7% top-1 accuracy and 5.36M parameters.

*Work done during an internship at Horizon Robotics.

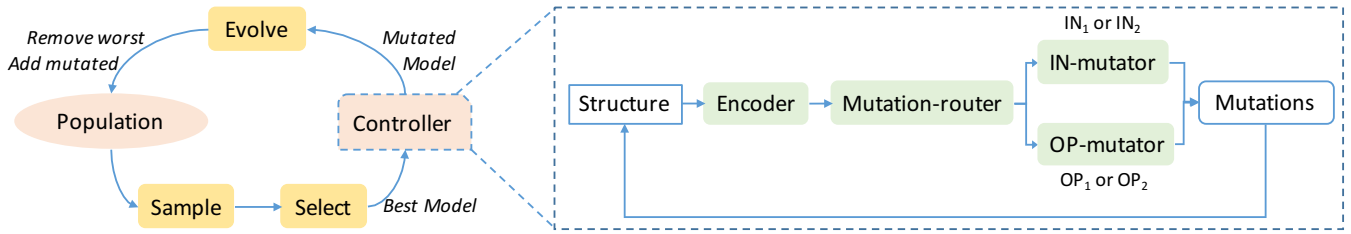


Figure 1: The evolutionary neural architecture search framework and the structure of the reinforced mutation controller.

Related Work

In this section, we describe RL-based and EA-based NAS and some techniques to search efficiently. Finally, we introduce some previous works on the integration of RL and EA and explain inner reasons for the integration in our method.

RL-based NAS

Reinforcement learning is prevalent in recent works (Zoph et al. 2017; Cai et al. 2018; Zoph and Le 2016; Zhong et al. 2018; Baker et al. 2016). In NAS (Zoph and Le 2016), neural networks are specified by a variable-length string which is generated by a RNN controller. The network specified by the string is then trained to return a validation accuracy. In turn, the controller is updated with policy gradient using the accuracy as reward. In this framework, networks specified by strings are generated layer by layer. The success reported by NAS (Zoph and Le 2016) inspires many other valuable works, but the expensive computational cost (28 days with 800 GPUs) also frightens some researchers. Training and evaluating a single model is time-consuming. In addition, training RL agents is sample-wise inefficient.

EA-based NAS

Evolution process in the nature is intuitively similar to NAS. Thus, many early automatic architecture search methods (Miller, Todd, and Hegde 1989; Yao and Liu 1997; Stanley and Miikkulainen 2002; Real et al. 2017; Miikkulainen et al. 2017; Xie and Yuille 2017) adopted EA, evolving a population of models. For instance, the large scale evolutionary method (Real et al. 2017) explores a CNN architecture space with neuro-evolution algorithm, which returns networks matching the human-designed models. The framework of our paper is based on AmoebaNets (Real et al. 2018), in which a common evolutionary algorithm, tournament selection strategy, matches or even outperforms its RL baseline (Zoph et al. 2017) in speed and accuracy. However, evolution process is a bit unstable due to the random mutation. To address this issue, we adopt a controller to make decisions for mutation and direct the evolution process.

Efficient NAS

Difficulties of NAS mainly come from the extremely large search space and the time-consuming model evaluation. In NASNet (Zoph et al. 2017), computational cost is saved with cell-wise search space, which is adopted by the following works (Real et al. 2018; Pham et al. 2018; Liu et al. 2017a).

Instead of exploring the whole network architecture, NAS-Net (Zoph et al. 2017) centers on learning a cell structure which is then stacked multiple times into a complete network, making the output networks scalable for various datasets and tasks. In addition, a variety of techniques on accelerating evaluation have proven effective: Block-QNN (Zhong et al. 2018) improves the search speed with an early-stop strategy. ENAS (Pham et al. 2018) utilizes parameters sharing among child models instead of training from scratch. EAS (Cai et al. 2018) utilizes the Net2Net transformation (Chen, Goodfellow, and Shlens 2015) to reuse parameters. Accuracy prediction, used in this work (Baker et al. 2018), is also a novel technique to save computational resources, although the accuracy predictor might not always be accurate enough.

Integration of EA and RL

RL has shown its capacity of accelerating evolutionary progress via Baldwinian or Lamarckian mechanisms (Downing 2001a). The idea of Integration RL and EA has been previously investigated, but our method is distinctly different from previous works. In (Downing 2001b), RL is used to enhance standard tree-based genetic programming in maze problems. In (Kamio and Iba 2005), integration of EA and RL is used to improve the adaption actions of a real robot. In (Hitoshi 1998), EA is integrated into a multi-agent Q-learning to shrink the search space.

In our method, a mutation controller is integrated into the evolution framework to learn the effects of modifications and make reasonable mutation actions. This integration brings us the following benefits:

- Search becomes more stable with the help of the reinforced mutation controller. Model architectures and their fitnesses (validation accuracies) are previously neglected but valuable hints generated during evolution. They are useful supervisory signals to train the mutation controller. It in turn eliminates the accumulation of harmful mutation.
- RL training becomes more efficient. Because making modifications to a network needs much fewer actions to make than constructing a model layer by layer. As the child model is modified from the parent model, the mutation controller is easy to learn the effects of slight differences between them.
- Training and evaluating a new model becomes more efficient. As differences between the child model and its parent exist merely in the mutated layers, the child could inherit most parameters from its parent model. This saves much resources from training the child model from scratch.

Methods

In this section, we introduce our method in three dimensions: search space, search strategy and training procedure. Search space is first described from block and cell to network. After that, we introduce the search strategy with the evolution framework and the details of the reinforced mutation controller. Finally, we explain the training procedure for the controller, child models and architectures deriving.

Search Space

Rather than designing the entire convolutional network, we adopt the idea that learning cell structures (Zoph et al. 2017). But our search space is a bit different from NASNet (Zoph et al. 2017). In this section, we introduce the search space by factorizing *network* into *cell* and *block*.

Block maps two inputs into one output feature map as shown in Figure 2 (b). It takes two input feature maps IN_1, IN_2 , applies two operators to them respectively and then combines them into a output feature map F_b via element-wise addition. For this reason, each block could be specified by a sequence of 4 numbers, IN_1, IN_2, OP_1, OP_2 . Moreover, if we take the combination operation, i.e., element-wise addition, into consideration, each block is defined as a string of 5 tokens, $IN_1, IN_2, OP_1, OP_2, A$. IN_1 and IN_2 are selected from $\{F_1^c, F_2^c, \dots, F_{b-1}^c, F_B^{c-1}, F_B^{c-2}\}$. F_1^c, \dots, F_{b-1}^c are outputs of previous blocks in the cell and F_B^{c-1}, F_B^{c-2} are outputs of the first and second previous cells. OP_1 and OP_2 are selected from a set of 6 functions:

3x3 depth-wise separable convolution,
5x5 depthwise-separable convolution,
7x7 depth-wise separable convolution,
3x3 avg pooling, 3x3 max pooling, identity.

Cell can be represented as a directed acyclic graph which consists of $\#B$ blocks. Taking a feature map with shape $H \times W \times F$ as input, cells with stride 2 output features with shape $\frac{H}{2} \times \frac{W}{2} \times 2F$ while cells with stride 1 do not change the shape of feature maps. $\#B$ blocks constitute one cell. Therefore, we search for the structure of each block and how they connect together to build a cell.

Network could be specified with three factors: the cell structure, $\#N$ the number of cells to be stacked and $\#F$ the number of filters in the first layer. As we fix $\#N$ and $\#F$ during search, our search space is constrained to all possible cell structures. Once search finished, models are constructed with different sizes to fit various tasks or datasets. We adjust the number of cells repeated $\#N$ and the number of filters in the first layer to control the depth and width of networks. As illustrated in Figure 2 (a), the architecture for ImageNet has two more cells with stride 2 and a deeper steam.

Each network therefore is specified with $5\#B$ tokens, $4\#B$ of which are variable during search. Therefore, searching network architecture is converted to search for $4\#B$ variables. This search space is slightly smaller than NASNet search space (Zoph et al. 2017). We use only one cell type and reduce the feature map size using cells with stride 2. Besides we use 6 candidate functions and fix combiners as element-wise addition. The complexity of the search space can be

Algorithm 1: Reinforced Evolutionary for Neural Architecture Search

input : num blocks each cell $\#B$, max num epochs $\#E$,
num filters in first layer $\#F$, num cells in model
 $\#N$, population size $\#P$, sample size $\#S$,
training set D_{train} , validation set D_{val}

output : a population of models P

```

1  $P^{(0)} \leftarrow \text{initialize}(\#F, \#N, \#P)$ 
2 for  $i=1:\#E$  do
3    $S^{(i)} \leftarrow \text{sample}(P^{(i-1)}, \#S)$ 
4    $B, W \leftarrow \text{select}(S^{(i)})$ 
5    $C, \omega^B \leftarrow \text{reinforced-mutate}(B)$ 
6    $\omega^C \leftarrow \text{finetune}(C, \omega^B, D_{train})$ 
7    $f_C \leftarrow \text{evaluate}(C, \omega^C, D_{val})$ 
8    $P^{(i)} \leftarrow \text{add-remove}(P^{(i-1)}, C, f_C, W)$ 
9 end
```

estimated with ease. Each block consists of 2 nodes. For each node we need to select its input from $b+1$ possible indexes and its operator from these 6 functions. As we set $\#B=5$, there are $(|S|^{\#B} \times (\#B+1)!)^2 = (6^5 \times (5+1)!)^2 = 3.1 \times 10^{13}$ possible networks, which is still an extremely large space.

Search Strategy

Evolution Framework To search for architectures with high performance automatically, a population of models P is initialized randomly. Each *individual* of P is trained on the training set D_{train} and evaluated on the validation set D_{val} . Its fitness f is defined as the validation accuracy. At each evolutionary step, a subset S is randomly sampled from P . According to their fitnesses, the best individual B and the worst individual W are selected among S . W is excluded from P and B becomes a *parent* to produce a child C with *mutation*. C is then trained and evaluated to measure its fitness f_C . Afterwards C is put back into P . This scheme actually belongs to *tournament selection* (Goldberg and Deb 1990), repeating competitions in random samples. The procedure is formulated in Algorithm 1.

Reinforced Mutation Reinforced mutation is implemented with a mutation controller to learn the effects of slight modifications and make mutation actions. Figure 1 shows the framework of our controller, which implements a mechanism of attention. The controller takes a string of $5\#B$ length which represents the given cell architecture. Specifically, our controller consists of 4 parts: (1) an Encoder (ENC) following an embedding layer to learn the effect of each part of the cell, (2) a Mutation-router (MUT-RT) to choose one from IN_1, IN_2, OP_1, OP_2 of the block, (3) an Input-mutator (IN-MUT) to change node's input with a new input IN_n (4) an OP-mutator (OP-MUT) to change node's operator with a new operator OP_n .

Encoder ENC is a bidirectional recurrent network with an input embedding layer. Hidden states learnt by ENC indicate the effect of a local part on the whole network. For block b in ENC, its hidden states are $H_{IN_1}^b, H_{IN_2}^b, H_{OP_1}^b, H_{OP_2}^b$ and H_A^b where $H_{OP_1}^b$ represents the effect of block b 's OP_1 on the

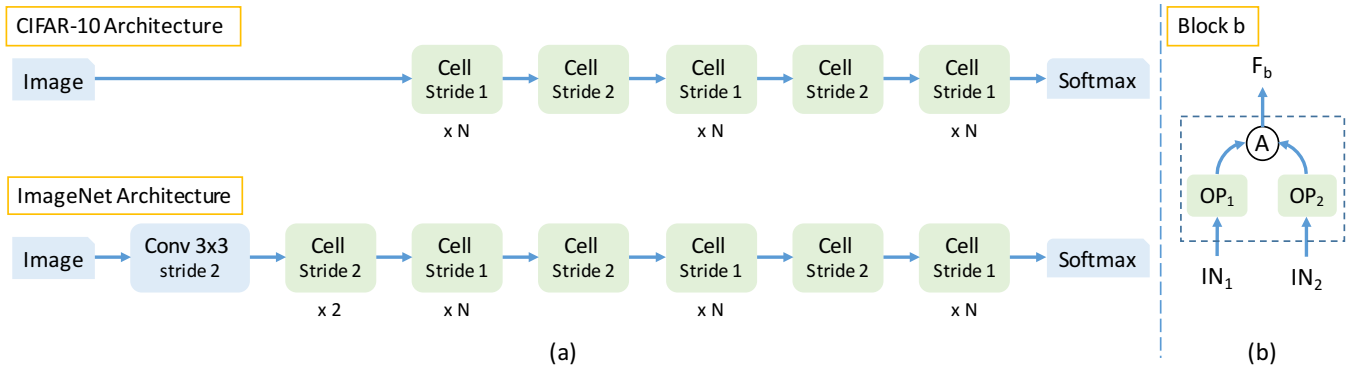


Figure 2: (a) Architectures employed for CIFAR-10 and ImageNet datasets respectively. During searching, the network structure is specified by the cell structure. The ImageNet architecture has an additional 3×3 convolution layer with stride 2 and two more cells with stride 2. (b) Each cell consists of $\#B$ blocks. Each block takes in two inputs (IN_1, IN_2), apply specific operations (OP_1, OP_2) to them respectively and then combine them with element-wise addition A to generate a feature map F_b . We search for IN_1, IN_2, OP_1, OP_2 for $\#B$ blocks to construct a reasonable cell structure, which in turn constitutes a network.

whole network. As each model is specified by $5\#B$ numbers, Enc generates $5\#B$ hidden states each step. Besides, we initialize two begin states, H^{c-1}, H^{c-2} , which represent the information of the first and second previous cells.

For block b , the controller makes two decisions sequentially. At first, depending on $H_{IN_1}^b, H_{IN_2}^b, H_{OP_1}^b, H_{OP_2}^b$, Mut-rt decides which one of IN_1, IN_2, OP_1, OP_2 in block b needs to be modified. It is sampled with a mechanism of attention via softmax classifiers. If an input index, IN_1 or IN_2 , is chosen, the IN-mut would be activated to pick one from $\{F_1^c, \dots, F_{b-1}^c, F_B^{c-1}, F_B^{c-2}\}$. Otherwise OP-mut would choose a new operator from the function set shown in . As there are B blocks in each cell, this process would be repeated for B times to modify a given architecture. Thus it makes $2\#B$ modification actions for each model. We describe the implementation details in the following.

Mutation-router Mut-rt is designed to find which ingredient of each block needs modification. For each block, Mut-rt's inputs are a subset of Enc's outputs $H_{IN_1}^b, H_{IN_2}^b, H_{OP_1}^b, H_{OP_2}^b$ and its output is one of IN_1, IN_2, OP_1, OP_2 , an ID to mutate. Equation (1) and (2) show this process: we apply a fully connected layer to each hidden state with parameter θ_{Mut-rt} , use *softmax* to compute the modification probability of each ingredient $P_{IN_1}^b, P_{IN_2}^b, P_{OP_1}^b, P_{OP_2}^b$ and sample one from IN_1, IN_2, OP_1, OP_2 with these probabilities.

IN-mutator IN-mut chooses a new input for the node, if $ID \in (IN_1, IN_2)$. Its inputs include the chosen ID 's hidden state H_{ID}^b , the hidden states of all previous block's outputs $[H_A^1, \dots, H_A^{b-1}]$, and the hidden states of previous and previous-previous cells H^{c-1}, H^{c-2} . Equation (3) and (4) show this process: we concat each of $H_{ID}^b, [H_A^1, \dots, H_A^{b-1}, H^{c-1}, H^{c-2}]$ with H_{ID}^b and apply a fully connected layer to them with parameter θ_{IN-mut} . Similar to Mut-rt, we use *softmax* to compute the probability of replacing the original input with each substitute and then we sample IN_n from $1 \dots b-1, c-1, c-2$ with these probabilities.

OP-mutator OP-mut outputs a new operator OP_n de-

Algorithm 2: Mutation generated by Controller

input : num blocks each cell $\#B$, a sequence a of 4 $\#B$ number specifying a cell
output : a sequence of mutation actions m

```

1  $H^{c-1}, H^{c-2} \leftarrow \text{Enc.begin}()$ 
2  $H^1, \dots, H^B \leftarrow \text{Enc}(H^{c-1}, a)$ 
3 for  $b=1:\#B$  do
4    $H_{IN_1}^b, H_{IN_2}^b, H_{OP_1}^b, H_{OP_2}^b, H_A^b \leftarrow H^b$ 
5    $ID \leftarrow \text{Mut-rt}([H_{IN_1}^b, H_{IN_2}^b, H_{OP_1}^b, H_{OP_2}^b])$ 
6   if  $ID \in (IN_1, IN_2)$  then
7      $IN_n \leftarrow \text{IN-mut}$ 
7      $(H_{ID}^b, [H_A^1, \dots, H_A^{b-1}, H^{c-1}, H^{c-2}])$ 
8      $m^{(b)} \leftarrow (ID, IN_n)$ 
9   else
10     $OP_n \leftarrow \text{OP-mut}(H_{ID}^b)$ 
11     $m^{(b)} \leftarrow (ID, OP_n)$ 
12  end
13 end

```

pending on the input H_{ID}^b . This process is simple and similar to Mut-rt as in Equation (5).

$$[P_{IN_1}^b, P_{IN_2}^b, P_{OP_1}^b, P_{OP_2}^b] = \text{softmax}(fc([H_{IN_1}^b, H_{IN_2}^b, H_{OP_1}^b, H_{OP_2}^b]; \theta_{Mut-rt})) \quad (1)$$

$$ID = \text{argmax}([P_{IN_1}^b, P_{IN_2}^b, P_{OP_1}^b, P_{OP_2}^b]) \quad (2)$$

$$[P_A^1, \dots, P^{c-1}, P^{c-2}] = \text{softmax}(fc(H_{ID}^b, [H_A^1, \dots, H_A^{b-1}, H^{c-1}, H^{c-2}]; \theta_{IN-mut})) \quad (3)$$

$$IN_n = \text{argmax}([P_A^1, \dots, P_A^{b-1}, P^{c-1}, P^{c-2}]) \quad (4)$$

$$OP_n = \text{argmax}(\text{softmax}(fc(H_{ID}^b))) \quad (5)$$

Training Procedure

In this section, we introduce procedures for training controller, training child models and deriving architectures.

Controller At each evolutionary step, the controller makes a sequence of mutation actions. Then a child model C is produced with the parent model modified. Then the validation accuracy f_C is computed with a parameters inheriting technique which is introduced in the following paragraph. The reward is a nonlinear function (Cai et al. 2018) of f_C , e.g. $Reward = \tan(f_C \times \frac{\pi}{2})$, since the gain of improving accuracy should be larger while the validation accuracy of its parent is higher. The controller parameters θ is updated via policy gradient.

Child Models Child models are trained and evaluated with its parameters inherited from their parents. For each alive model B in the population, we store its architecture string, its fitness f_B and its learnable parameters ω^B . As each child model C is generated from its parent model with slight modifications, differences between them only exist in the mutated layers. Therefore the child could inherit most parameters from the parent B . ω^C are classified into inheritable parameters ω_{inh}^C and new initialized parameters ω_{new}^C . And its fitness (validation accuracy) f_C could be evaluated with fine-tuning instead of training from scratch. During fine-tuning, we train ω^C on a whole pass through D_{train} with the learning rate of ω_{new}^C 10 times that of ω_{inh}^C . In the experiments, the learning rate of ω_{new}^C equals to 0.01.

Deriving Architectures During search, we set each cell contains $\#B=5$ blocks, and $\#F=24$ filters in the first convolution cell and we unroll the cells for $\#N=2$. After the maximum number of epochs $\#E$ is reached, we only retrain the models in the population from scratch and then take the model with highest accuracy. It is possible to improve our results by retraining more sampled models from scratch as done by other works (Zoph et al. 2017; Zoph and Le 2016), but it is unfair to prove the performance of our controller. In the experiments, the population size $\#P$ is set as 20. For better comparison, we set $\#F$ and $\#N$ same to NASNets(Zoph et al. 2017).

Experimental Results

In this section, we first show our implementation details. Then, we compare our best architecture RENASNet with both state-of-the-art hand-design networks and other searched models on CIFAR-10 and ImageNet datasets. The best model we discovered is RENASNet in Figure 3 After that, we make ablation studies to show search efficiency and stability of RENAS. For search efficiency, we compare RENAS with other state-of-the-art NAS methods to show the overall efficiency and compare it with our evolutionary baseline to show that reinforced evolution is more efficient. For search stability, we conduct the ablation study under two situations, fixed initialization and various initialization, to eliminate the influence of initialization.

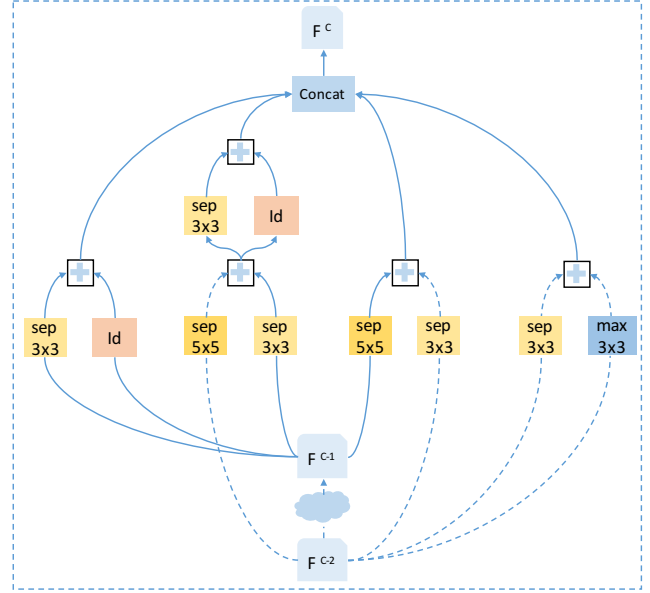


Figure 3: The best cell we obtained

Implementation Details

Dataset for Architecture Search We conduct our search method on CIFAR-10 dataset (Krizhevsky and Hinton 2009), which consists of 50,000 training images and 10,000 test images. We partition 5,000 images from the training set as a validation set. We use standard data pre-processing and augmentation steps. All images are whitened with the channel mean subtracted and the channel standard deviation divided. And then we crop 32 x 32 patches from images padded to 40 x 40 and randomly flip them horizontally.

Training details on CIFAR-10 When training models on CIFAR-10, we use standard SGD optimizer with momentum rate set to 0.9, auxiliary classifier located at $\frac{2}{3}$ of the maximum depth weighted by 0.4, weight decay $2e-4$, and dropout of 0.2 in the final softmax layer. In addition, we drop each path with probability 0.4 for regularization. Our batch size is 36 on each GPU and we use 4 GPUs. Initial learning rate is 0.05 and it decays with a cosine restart schedule.

Training details on ImageNet We train models on mobile ImageNet for 200 epochs, using standard SGD optimizer with momentum rate set to 0.9, auxiliary classifier located at $\frac{2}{3}$ of the maximum depth weighted by 0.4, weight decay $4e-5$. Our batch size is 64 on each GPU and we use 4 GPUs. Initial learning rate is 0.1 and it decays in a polynomial schedule.

Details of the Controller For our controller, we use an LSTM with an embedding layer, and the embedding size and the hidden state size of LSTM are both 100. The parameters of our controller are initialized with random values sampled from a normal distribution with a mean of zero and standard deviation of 0.01 and trained with Adam at a learning rate of 0.001. We apply a tanh constant of 2.5 and a temperature of 5.0 to the logits of the controller, and add the entropy of the controller to the reward with 0.1 weighted.

Table 1: CIFAR-10 results. The top section presents the top hand-design networks, the middle section presents other architecture search results and the bottom section shows our results. **#Params** means the number of free parameters.

Model	GPUs	Days	#Params	Error(%)	Method
DenseNet-BC (Huang et al. 2017)	-	-	25.6M	3.46	-
PNASNet-5 (Liu et al. 2017a)	100	1.5	3.2M	3.41 ± 0.09	SMBO
NASNet-A + cutout (Zoph et al. 2017)	500	4	3.3M	2.65	RL
AmoebaNet-B + cutout (Real et al. 2018)	450	7	2.8M	2.55 ± 0.05	EA
Block-QNN-S + cutout (Zhong et al. 2018)	32	3	6.1M	3.30	RL
ENAS + cutout (Pham et al. 2018)	1	0.5	4.6M	2.89	RL
RENASNet (6, 32) + cutout	4	1.5	3.5M	2.98 ± 0.08	EA&RL

Table 2: ImageNet classification results in the mobile setting. The results of hand-design models are in the top section, other NAS results are presented in the middle section and the result of our model is in the bottom section.

Model	#Params	#Mult-Adds	Top-1/Top-5 Acc(%)	Method
MobileNet-v1 (Howard et al. 2017)	4.2M	569M	70.6 / 89.5	-
MobileNet-v2 (1.4)(Sandler et al. 2018)	6.9M	585M	74.7 / -	-
ShuffleNet-v1 2x (Zhang et al. 2017)	≈ 5 M	524M	73.7 / -	-
ShuffleNet-v2 2x (Ma et al. 2018)	≈ 5 M	591M	74.9 / -	-
NASNet-A (Zoph et al. 2017)	5.3M	564M	74.0 / 91.6	RL
NASNet-B (Zoph et al. 2017)	5.3M	488M	72.8 / 91.3	RL
NASNet-C (Zoph et al. 2017)	4.9M	558M	72.5 / 91.0	RL
AmoebaNet-A (Real et al. 2018)	5.08M	555M	74.5 / 92.0	EA
AmoebaNet-B (Real et al. 2018)	5.29M	555M	74.0 / 91.5	EA
AmoebaNet-C (Real et al. 2018)	5.06M	535M	75.1 / 92.1	EA
AmoebaNet-C (more filters) (Real et al. 2018)	6.35M	570M	75.7 / 92.4	EA
PNASNet-5 (Liu et al. 2017a)	5.1M	588M	74.2 / 91.9	SMBO
ENAS (Pham et al. 2018)*	5.1M	523M	74.3 / 91.9	RL
RENASNet (4, 44)	5.36M	580M	75.7 / 92.6	EA&RL

* The result of ENAS was obtained by training with our setup, as it is not reported in (Pham et al. 2018).

Results on CIFAR-10

Here we present the performance of our final model, RENASNet, and make a comparison to other state-of-the-art models in Table 1. After the cell structures are fixed, we construct the entire networks same to the structure setting of NASNet(Zoph et al. 2017) and train them with the details mentioned before. The simple notation (6,32) denotes cell unroll for $N = 6$ times and $F = 32$ filters in the first convolution cell.

Results on ImageNet

State-of-the-art image classifiers on ImageNet is shown in Table 2. We conduct the comparison in the mobile setting where image size is 224x224 and the number of multi-add operations is under 600M. Note that as the accuracy of ENAS(Pham et al. 2018) on ImageNet is not reported in the original paper, we trained it with all hyper-parameters and setup exactly same to RENASNet.

Results Analysis

The CIFAR-10 results are presented in Table 3. RENASNet achieves a comparable results with other state-of-the-art models while using much less computational resources than NASNet (500 GPUs over 4 days) and AmoebaNet (450 GPUs

over 7 days). ENAS is more efficient than our method, but our model has one fourth less parameters with similar accuracy.

The results on ImageNet are more convincing because CIFAR-10 is small and easy to be over-fitting. The mobile setting ImageNet results are shown in Table 1. RENASNet surpasses both the manually designed models, including MobileNets (Howard et al. 2017; Sandler et al. 2018) and ShuffleNets (Zhang et al. 2017; Ma et al. 2018), and the other state-of-the-art auto-designed models.

Search Efficiency

In this section, we show the search efficiency of RENAS on CIFAR-10 with ablation studies. We first compare the efficiency of RENAS with other state-of-the-art NAS methods in Table 3. After that, we compare it with Baseline EA to show that the efficiency gains in Figure 4.

The search efficiency comparison according to the total number of SGD process is shown in Table 3. **#M** means the number of models trained during search, and **#Ex** means the number of examples used to train each model. **Cost** is the total number of examples processed through SGD during search. This metric is first used in PNAS (Liu et al. 2017a). In terms of the number of models **#M** trained during search, RENAS needs much less models than NASNet (Zoph et al.

Table 3: Search Efficiency of different NAS methods.

	#M	#Ex	Cost
NASNet(Zoph et al. 2017)	20000	0.9M	18B
AmoebaNet-A(Real et al. 2018)	20000	1.13M	22.6B
Hier-EA(Liu et al. 2017b)	7000	5.12M	35.8B
PNASNet-5(Liu et al. 2017a)	1160	0.9M	1.0B
EAS(Cai et al. 2018)	450	0.9M	405M
RENAS	4000	45K	180M

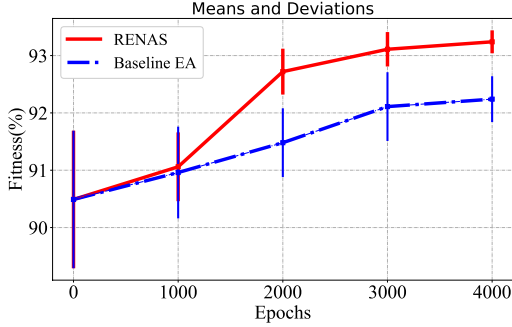


Figure 4: The mean and deviation curve of the models' fitnesses in the population. RENAS helps the population evolves in a more efficient way and converge in a better ends.

2017) and AmoebaNet-A (Real et al. 2018). It shows that RENAS converges faster than these two state-of-the-art RL-based and EA-based NAS methods. In terms of **Cost**, RENAS uses the least computational cost, thanks to the parameter inheritance technique.

Search efficiency and effectivity gains are shown in Figure 4. The curves show the means and standard deviations of the population's fitnesses during search. The Baseline EA is identical to RENAS except that its mutation is random. We keep track of the models in the population for every 1000 epochs. Each child model snapshot is re-trained from scratch using the training set for 100 epochs on CIFAR-10 with initial learning rate 0.025 and a cosine schedule down to zero. It shows our method increases the growth rate and the deviation decreases faster than our baseline. And the population of RENAS evolves to a better status in fewer epochs.

Search Stability

Ablation experiments are performed to test the search stability of RENAS on CIFAR-10. The Baseline EA is also identical to RENAS except that its mutation is random. Figure 5 shows three search stability levels for EA-based NAS. Each sub-figure is one experiment instance of search process.

- **Success:** the left scatter shows one instance of RENAS process where model fitnesses increase gradually and converge in the final stage.
- **Fail:** the right scatter shows the situation that the search collapses because of accidental unreasonable mutation accumulation.
- **Unstable:** the situation shown in the middle is a intermediate state, fluctuating between Success and Fail.

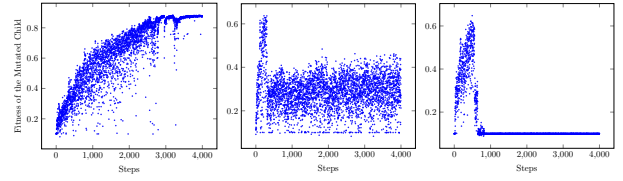


Figure 5: EA-based NAS stability levels. *Left: Success Middle: Unstable Right: Fail*

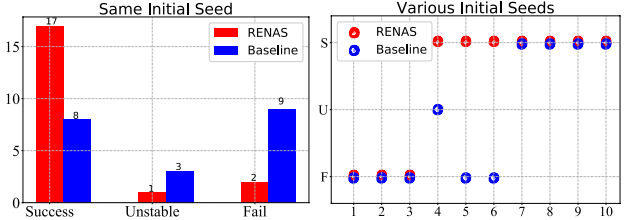


Figure 6: Search stability comparisons in two situations. *Left:* Fixed initialization comparison for 20 groups with the same initialization seed. RENAS succeeds to search in 17 groups while Baseline EA succeeds in only 8 groups. *Right:* Initialization various comparison for 10 groups with 10 different initialization seeds. RENAS succeeds in 7 groups while Baseline EA succeeds in only 4 groups.

We repeat running RENAS and Baseline EA for 30 groups in total and count the number of occurrences of each situation. In the first 20 groups, we fix the random seed to ensure that it evolves from the same initial population each time. In the other 10 groups, we uses 10 different initialization seeds.

Search stability comparison is shown in Figure 6. In Figure 6 *Left*, Baseline EA successfully finishes search for less than half times while RENAS only fails or becomes unstable for 3 times. It empirically shows that RENAS has a much better search stability and a higher success rate. In Figure 6 *Right*, it shows that the quality of initializations indeed affects stability, but RENAS is still more stable. Baseline EA becomes unstable in 1 group and fails in 5 groups while RENAS succeeds to search in most groups. Evolution algorithm is instinctively sensitive to initializations. But RENAS survives in some terrible initializations and alleviates the influence of initializations. The best cell structure shown in Figure 3 is obtained from one of the success search of RENAS.

Conclusion

We combined evolution algorithm and reinforcement learning in a single framework for neural architecture search. Inspired by the procedure of designing networks manually, we use a controller to learn the effects of modifications and make better mutation actions. Our method improves both the search stability and efficiency with previously neglected but valuable information. The resulting models achieve competitive performance on CIFAR-10 and outperforms other state-of-the-art models on mobile ImageNet. In the future, we would like to directly apply RENAS to other computer vision tasks, e.g., object detection.

References

- Baker, B.; Gupta, O.; Naik, N.; and Raskar, R. 2016. Designing neural network architectures using reinforcement learning. *arXiv preprint arXiv:1611.02167*.
- Baker, B.; Gupta, O.; Raskar, R.; and Naik, N. 2018. Accelerating neural architecture search using performance prediction. *arXiv preprint arXiv:1705.10823*.
- Cai, H.; Chen, T.; Zhang, W.; Yu, Y.; and Wang, J. 2018. Efficient architecture search by network transformation. In *AAAI*, 1–8.
- Chen, T.; Goodfellow, I. J.; and Shlens, J. 2015. Net2net: Accelerating learning via knowledge transfer. *arXiv preprint arXiv:1511.05641*.
- Downing, K. L. 2001a. Adaptive genetic programs via reinforcement learning. In *GEC*, 19–26.
- Downing, K. L. 2001b. Reinforced genetic programming. *Genetic Programming and Evolvable Machines* 2(3):259–288.
- Goldberg, D. E., and Deb, K. 1990. A comparative analysis of selection schemes used in genetic algorithms. In *FGA*, 69–93.
- He, K.; Zhang, X.; Ren, S.; and Sun, J. 2016. Deep residual learning for image recognition. In *CVPR*, 770–778.
- Hitoshi, I. 1998. Multi-agent reinforcement learning with genetic programming. In *GP*, 167–167.
- Howard, A. G.; Zhu, M.; Chen, B.; Kalenichenko, D.; Wang, W.; Weyand, T.; Andreetto, M.; and Adam, H. 2017. Mobilenets: Efficient convolutional neural networks for mobile vision applications. *arXiv preprint arXiv:1704.04861*.
- Huang, G.; Liu, Z.; van der Maaten, L.; and Weinberger, K. Q. 2017. Densely connected convolutional networks. In *CVPR*, 2261–2269.
- Kamio, S., and Iba, H. 2005. Adaptation technique for integrating genetic programming and reinforcement learning for real robots. *IEEE Trans. Evolutionary Computation* 9(3):318–333.
- Krizhevsky, A., and Hinton, G. 2009. Learning multiple layers of features from tiny images. *Technical report*. 1(4):1–7.
- Krizhevsky, A.; Sutskever, I.; and Hinton, G. E. 2012. ImageNet classification with deep convolutional neural networks. In *NIPS*, 1106–1114.
- Liu, C.; Zoph, B.; Shlens, J.; Hua, W.; Li, L.; Fei-Fei, L.; Yuille, A. L.; Huang, J.; and Murphy, K. 2017a. Progressive neural architecture search. *arXiv preprint arXiv:1712.00559*.
- Liu, H.; Simonyan, K.; Vinyals, O.; Fernando, C.; and Kavukcuoglu, K. 2017b. Hierarchical representations for efficient architecture search. *arXiv preprint arXiv:1711.00436*.
- Ma, N.; Zhang, X.; Zheng, H.; and Sun, J. 2018. Shufflenet V2: practical guidelines for efficient CNN architecture design. *arXiv preprint arXiv:1807.11164*.
- Miikkulainen, R.; Liang, J. Z.; Meyerson, E.; Rawal, A.; Fink, D.; Francon, O.; Raju, B.; Shahrzad, H.; Navruzian, A.; Duffy, N.; and Hodjat, B. 2017. Evolving deep neural networks. *arXiv preprint arXiv:1703.00548*.
- Miller, G. F.; Todd, P. M.; and Hegde, S. U. 1989. Designing neural networks using genetic algorithms. In *ICGA*, 379–384.
- Pham, H.; Guan, M. Y.; Zoph, B.; Le, Q. V.; and Dean, J. 2018. Efficient neural architecture search via parameter sharing. *arXiv preprint arXiv:1802.03268*.
- Real, E.; Moore, S.; Selle, A.; Saxena, S.; Suematsu, Y. L.; Tan, J.; Le, Q. V.; and Kurakin, A. 2017. Large-scale evolution of image classifiers. 2902–2911.
- Real, E.; Aggarwal, A.; Huang, Y.; and Le, Q. V. 2018. Regularized evolution for image classifier architecture search. *arXiv preprint arXiv:1802.01548*.
- Sandler, M.; Howard, A. G.; Zhu, M.; Zhmoginov, A.; and Chen, L. 2018. Inverted residuals and linear bottlenecks: Mobile networks for classification, detection and segmentation. *arXiv preprint arXiv:1801.04381*.
- Simonyan, K., and Zisserman, A. 2014. Very deep convolutional networks for large-scale image recognition. *arXiv preprint arXiv:1409.1556*.
- Stanley, K. O., and Miikkulainen, R. 2002. Evolving neural networks through augmenting topologies. *Evolutionary computation* 10(2):99–127.
- Szegedy, C.; Liu, W.; Jia, Y.; Sermanet, P.; Reed, S. E.; Anguelov, D.; Erhan, D.; Vanhoucke, V.; and Rabinovich, A. 2015. Going deeper with convolutions. In *CVPR*, 1–9.
- Szegedy, C.; Vanhoucke, V.; Ioffe, S.; Shlens, J.; and Wojna, Z. 2016. Rethinking the inception architecture for computer vision. In *CVPR*, 2818–2826.
- Szegedy, C.; Ioffe, S.; Vanhoucke, V.; and Alemi, A. A. 2017. Inception-v4, inception-resnet and the impact of residual connections on learning. In *AAAI*, 4278–4284.
- Xie, L., and Yuille, A. L. 2017. Genetic CNN. 1388–1397.
- Yao, X., and Liu, Y. 1997. A new evolutionary system for evolving artificial neural networks. *IEEE Trans. Neural Networks* 8(3):694–713.
- Zhang, X.; Zhou, X.; Lin, M.; and Sun, J. 2017. Shufflenet: An extremely efficient convolutional neural network for mobile devices. *arXiv preprint arXiv:1707.01083*.
- Zhong, Z.; Yan, J.; Wu, W.; Shao, J.; and Liu, C.-L. 2018. Practical block-wise neural network architecture generation. In *CVPR*, 2423–2432.
- Zoph, B., and Le, Q. V. 2016. Neural architecture search with reinforcement learning. *arXiv preprint arXiv:1611.01578*.
- Zoph, B.; Vasudevan, V.; Shlens, J.; and Le, Q. V. 2017. Learning transferable architectures for scalable image recognition. *arXiv preprint arXiv:1707.07012*.